

OPTICAL PROPERTIES OF LOWEST-ENERGY CARBON ALLOTROPES FROM THE FIRST-PRINCIPLES CALCULATIONS

V.A. Saleev* and A.V.Shipilova†

*Samara National Research University,
Moscow Highway, 34, 443086, Samara, Russia*

Abstract

We study the optical properties of lowest-energy carbon allotropes in the infrared, visible and ultra-violet ranges of light in the general gradient approximation of the density functional theory. In our calculations we used the all-electron approach as well as the pseudo-potential approximation. In the infrared range, the complex dielectric functions, infrared and Raman spectra have been calculated using CRYSTAL14 program. The electronic properties and energy-dependent dielectric functions in the visible and ultraviolet ranges have been calculated using VASP program. We have described with a good accuracy experimentally known optical properties of cubic diamond crystal. Using obtained set of relevant parameters for calculations, we have predicted optical constants, dielectric functions and Raman spectra for the lowest-energy hypothetical carbon allotropes and lonsdaleite.

Key words: optical properties, Raman spectrum, first-principles calculations, density functional theory, crystal structure, carbon allotropes.

PACS numbers: 61.50.Ah, 78.20.Bh

*Electronic address: saleev@samsu.ru

†Electronic address: alexshipilova@samsu.ru

I. INTRODUCTION

Diamond and different forms of carbon materials are the subject of the intensive theoretical and experimental study [1,2]. It is well known that carbon can form sp^2 and sp^3 hybridized bonds which are realized under ambient conditions in cubic diamond, graphite, fullerene and graphene [3]. At high temperature and pressure graphite can be converted to cubic diamond or to the lonsdaleite (2H hexagonal diamond) [4,5]. For a long time, hexagonal diamond has been produced artificially by static and shock wave compression of well-crystallized graphites [6]. Recently it was shown that hexagonal diamond can be also obtained from cubic diamond [7]. It was found that graphite cold-compression leads to a creation of the new sp^3 -bonded stable forms of carbon allotropes [8]. Nowadays, there are about two hundreds of different predicted hypothetical sp^3 carbon allotropes, which are collected in the SACADA database [9]. The small difference of energy of several these allotropes relatively to the diamond, 0.01 – 0.10 eV per atom, raises the idea of a possibility to find these allotropes in the mixed carbon phases. The experimental search of such carbon allotropes should be based on some new physical information about formation of these new phases. The most probable signals can be connected with optical properties of the materials, such as Raman spectra, optical coefficients in the regions of infrared (IR), visible and ultraviolet (UV) spectra, as well as the energy dependence of the absorption and refractive indices. Here we calculate different optical properties of the six lowest-energy sp^3 carbon allotropes: cubic diamond, lonsdaleite [4], 4H-diamond [10], SiC12 [11], C28 [12] and mtn [13]. The main goal of our study is to find the quantitative level of difference between optical properties of cubic diamond and relevant carbon allotropes which can be measured experimentally. We start with a prediction of Raman shift spectra and IR active mode spectra, than we will study energy-dependent complex dielectric functions and their derivative in the ranges of visible and ultraviolet light. Our calculations are based on density-functional-theory (DFT) methods [14,15] as it is implemented in CRYSTAL14 [16] and VASP [17] program packages. The calculations for the IR range have been done using CRYSTAL14 program, which uses the all-electron approach with atomic orbital basis sets. The relevant calculations in the visible and ultraviolet ranges of light have been done using VASP program package which uses plane-wave basis sets and the pseudo-potential approach.

II. COMPUTATIONAL METHODS AND DETAILS

Raman and IR spectra of crystal structure are defined by the set of harmonic phonon frequencies at the Γ point which can be obtained from the diagonalization of the Hessian matrix of the second derivatives with respect to atomic displacements [18]:

$$H_{ai,bj}^{\Gamma} = \frac{1}{\sqrt{M_a M_b}} \left(\frac{\partial^2 E}{\partial u_{ai} \partial u_{bj}} \right) \quad (1)$$

where u_{ai} and u_{bj} are displacements of atoms a and b in the reference cell along the i -th and j -th Cartesian directions, respectively. The Raman intensity of the Stokes line of a phonon mode Q_p , active due to the α_{ij} component of the polarizability tensor α , is expressed as follows:

$$I_{ij}^p \propto \left(\frac{\partial \alpha_{ij}}{\partial Q_p} \right)^2 \quad (2)$$

The scheme of calculation, recently implemented in the CRYSTAL14 program [16], explores second-order Coupled-Perturbed Hartree-Fock/Kohn-Sham (CPHF/KS) equations [19]. The Raman spectrum is then computed by considering the transverse optical (TO) modes and by adopting a pseudo-Voigt functional form: a linear combination of a Lorentzian and a Gaussian curve with full width at half maximum of 8 cm^{-1} . Raman intensities are normalized so that the largest value is conventionally set to 100 a.u. To calculate IR spectra we should know the complex dielectric tensor $\varepsilon_{ii}(\nu)$ which is computed for each inequivalent polarization direction on the basis of a classical Drude-Lorentz model:

$$\varepsilon_{ii}(\nu) = \varepsilon_{opt,ii} + \sum_p \frac{f_{p,ii} \nu_p^2}{\nu_p^2 - \nu^2 - i\nu\gamma_p} \quad (3)$$

where ii indicates the polarization direction, $\varepsilon_{opt,ii}$ is the optical dielectric tensor, ν_p , f_p and γ_p are the TO frequency, oscillator strength and damping factor for the p -th vibration mode, respectively. The real and imaginary parts of $\varepsilon_{ii}(\nu)$ are computed and the maxima of this function correspond to the TO frequencies. The optical or high-frequency dielectric tensor is computed in a quasi-free electron approximation via coupled perturbed Hartree-Fock (Kohn-Sham) method [20]. The refractive (n) and absorption (k) indices are computed as real and imaginary parts of the complex refractive index $n^*(\nu) = \sqrt{\varepsilon(\nu)}$, also for each inequivalent polarization direction.

In the projector augmented plane wave method realized in VASP the frequency-dependent dielectric functions is obtained in the random phase approximation, where the imaginary

part of the frequency-dependent dielectric tensor is written as

$$\varepsilon_{ij}^{(2)}(\omega) = \frac{4\pi^2 e^2}{\Omega} \lim_{q \rightarrow 0} \frac{1}{q^2} \sum_{c,v,k} 2w_k \delta(\epsilon_{ck} - \epsilon_{vk} - \omega) \langle u_{ck+e_{iq}} | u_{vk} \rangle \langle u_{ck+e_{jq}} | u_{vk} \rangle^* \quad (4)$$

where the indices c and v refer to conduction and valence band states respectively in the sum over the empty states, $\epsilon_{c,vk}$ are the corresponding eigenenergies, Ω is the volume of a primitive cell, k -point weights w_k are defined such that they sum to 1, $e_{i,j}$ are the unit vectors for the three Cartesian directions, and u_{ck} is the cell-periodic part of the orbitals at point k . The real part of the dielectric tensor $\varepsilon^{(1)}(\omega)$ is obtained by the Kramers-Kronig transformation

$$\varepsilon_{ij}^{(1)} = 1 + \frac{2}{\pi} P \int_0^\infty \frac{\varepsilon_{ij}^{(2)}(\omega') \omega' d\omega'}{\omega'^2 - \omega^2 + i\eta} \quad (5)$$

where P denotes the principal value. By cubic symmetry, the following relation is satisfied for diamond and *mtn* allotrope

$$\varepsilon_{xx}^{(1,2)} = \varepsilon_{yy}^{(1,2)} = \varepsilon_{zz}^{(1,2)}, \quad \varepsilon_{ij}^{(1,2)} = 0, i \neq j, \quad (6)$$

so the real and imaginary parts of the complex dielectric function $\varepsilon = \varepsilon_1 + i\varepsilon_2$ can be determined by $\varepsilon_{1,2} = \varepsilon_{xx}^{(1,2)}$. In the case of the other, anisotropic, structures we use the average values:

$$\varepsilon_{1,2} = \overline{\varepsilon_{1,2}} = \frac{1}{3} \left(\varepsilon_{xx}^{(1,2)} + \varepsilon_{yy}^{(1,2)} + \varepsilon_{zz}^{(1,2)} \right). \quad (7)$$

III. COMPUTATIONAL SETUP

A. CRYSTAL14

We use the two schemes of DFT calculations, both are implemented in the CRYSTAL14 program [16]. The first one incorporates the Perdew-Burke-Ernzerhof (PBE) exchange-correlation functional [21] at general gradient approximation (GGA) of DFT and POB-TZVP all-electron basis set [22], and the second one the B3LYP hybrid functional [23] and adopted Poples 6-21G Gaussian all-electron basis set [24,25]. The level of accuracy of calculating the energies of Coulomb and Hartree-Fock exchanges is controlled by a set of TOLINTEG parameters, which were chosen as {8, 8, 8, 8, 18}. The convergence threshold on energy for the self-consistent-field (SCF) calculations is 10^{-7} Hartree for structural optimization and 10^{-8} Hartree for vibration frequency calculations. The number of basis vectors

in the irreducible Brillouin zone is given by the shrink parameter $IS = 8$ for structural optimization and $IS=16$ for vibration frequency calculations. The relaxation of cell parameters and atomic positions to equilibrium values was carried out until the lattice stress became less than 0.02 GPa.

B. VASP

The computations of the complex dielectric functions in the visible and ultraviolet regions were performed by the VASP package [17] at the level of GGA and with two functionals: the above-mentioned PBE [21] and the screened Heyd, Scuseria, and Ernzerhof (HSE06) hybrid functional [26], since the latter is well-suited to reproduce the electronic properties including the band gaps of a number of elemental and binary insulators and semiconductors. For this purpose, at first we performed the relaxation of the discussed structures with a cutoff energy of 700 eV for the plane-wave basis set, until the energy was converged up 10^{-7} eV per unit cell and the residual stress was less than 10^{-5} eV per atom. The integration over the Brillouin zone was performed using Monkhorst-Pack grids with the number of k-points along each direction of the reciprocal cell equal to an integer divisor of 25 \AA over the length of corresponding lattice vector. The chosen set of input parameters gives the reliable results for the main physical properties of diamond as it was shown in our previous work [12].

IV. STRUCTURAL PROPERTIES

The full geometry optimization of studied structures have been performed using the quasi-Newton algorithm in CRYSTAL14 program. The relaxed lattice constants and atomic Wyckoff positions are presented in the Tables I and II. The differences between lattice constants obtained in two schemes of calculations are about 1 %. While the energy differences per atom relatively diamond are equal, see Tables III and IV. To check a mechanical stability of hypothetical allotropes under study, we calculated the elastic constants and phonon spectra which are collected in the Fig. 4. Our results for structural properties agree with previous DFT calculations [10-13].

V. RAMAN AND IR SPECTRA

Raman identification of new carbon allotropes needs a precise calculation of vibration spectra. We performed these calculations applying quasi-harmonic approximation at the point as it was done for Raman identification of lonsdaleite in Refs. [27,28] and for Raman spectroscopy of nanocrystalline diamond in Ref. [29]. We have found for cubic diamond that the position of single Raman peak, corresponding to the first-order scattering of F_{2g} symmetry, is 1297 cm^{-1} (PBE, POB-TZVP) and 1332 cm^{-1} (B3LYP, 6-21G). The last one is in a best agreement with experimental value. Such a way, we perform calculations of Raman and IR spectra here and after using B3LYP exchange-correlation functional and modified Poples 6-21 basis set [25]. The presented in Fig. 1 polycrystalline (powder) Raman spectra were computed by averaging over the all possible orientations of the crystallites.

For the lonsdaleite we predict three Raman active modes: E_{1g} (1336), A_{1g} (1312) and E_{2g} (1209). Up to now, the pure monocrystalline lonsdaleite have not been found or synthesized and there is a well-known problem of correct diagnostics of lonsdaleite phase within cubic diamond-lonsdaleite intergrowths. Possible attendance of nanocrystalline cubic diamond can be a reason of incorrect interpretation of Raman spectra in experimental study. It was found that the Raman modes dynamics under laser heating allows splitting of cubic diamond and lonsdaleite modes and recognize diamond polymorphs [28]. The measurements in the region of $1300\text{-}1340\text{ cm}^{-1}$ show the presence of two Raman active modes, A_{1g} (1319) and F_{1g} (1322). The control measurement for co-sized cubic diamond particles give downshift of a Raman active mode F_{2g} (1332) up to 1326 cm^{-1} . Taking into account this downshift effect, we can declare the agreement of our prediction with the experimental data for lonsdaleite [28] at least for two high-frequency modes. We also obtain a rough agreement with recent measurements of Ref. [29], in which the most intensive band at $1292\text{-}1303\text{ cm}^{-1}$ and at $1219\text{-}1244\text{ cm}^{-1}$ are interpreted as contributions from A_{1g} and E_{2g} vibration modes of lonsdaleite phase in Popigai impact rock. Early DFT calculations, performed in the local density approximation (LDA), gave the following results: E_{1g} (1312), A_{1g} (1305), E_{2g} (1193) [30] and E_{1g} (1338), A_{1g} (1280), E_{2g} (1221) [31].

In Fig. 1(a-e), we present our results for polycrystalline (powder) Raman spectra with intensity plotted in arbitrary units. Of course, it has the dependence on direction for monocrystalline structures, but it is small and we discuss it later for real refractive in-

dices only. The single peak of cubic diamond corresponding $F_{2g}(1332)$ mode is shown in all figures for comparison. The number of active Raman modes or peaks depends on symmetry of crystal lattice and on the number of non-equivalent atoms in the asymmetric unit. As we see, quantum-mechanical approach predicts a very specific Raman spectrum for every allotrope, which can be considered as finger prints of these structures in the experimental search. The improvement of experimental methods to the level of accuracy of theoretical calculations will be crucial for search and recognition of diamond polymorphs.

The high-frequency refractive indices for different direction (ii=xx, yy, zz), accordingly Vogt notation, are collected in the Table V. The calculation with PBE functional and POB-TZVP basis set gives answer which is very close to the experimental value for cubic diamond (2.40) instead of the calculation with B3LYP functional used successfully for Raman spectrum calculation. The refractive asymmetry factor can be defined as follows. The values of for lonsdaleite, C28, SiC12 and 4H-diamond are about 2.5-3.5 %. This is enough large values for experimental test and recognition. The list of calculated IR active modes which initiate absorption of light in IR region are presented in Table VI. The ideal cubic diamond and lonsdaleite crystals do not absorb IR light. It means that experimental viewing of absorption for diamond-like structures may be used for recognition of new sp^3 carbon allotropes.

VI. VISIBLE AND UV SPECTRA

Optical properties are immediately connected with the electronic band structure of the crystal. To calculate the interband and intraband electron optical transitions one needs to solve the band structure of the system and know its band gap in different symmetry points of reciprocal space. Because of this reason, we calculated the electronic band structure for all the allotropes under study (see Fig. 5) and collected to the table our results for indirect and direct (in Γ -point) band gaps for all the considered structures within PBE and HSE06 functionals (see Table VII). It is well-known that the former fails to reproduce the optical band gaps while the latter provides the reliable results. Our result of 5.38 eV band gap for diamond successfully reproduces the well-known experimental value of 5.47 eV [1].

Then, we calculated the complex dielectric function for diamond, lonsdaleite and considered lowest-energy allotropes in the random phase approximation as it was explained in the Sec. II. In the Figs. 2 and 3 we present our predictions for diamond obtained with

PBE exchange-correlation functional (bold solid line) and HSE06 functional (dashed line) together with experimental data (solid line) from the work [1] and PBE based predictions for lonsdaleite (dash-dotted line). We find a good agreement between theory and experiment within PBE functional calculations in the position and highness of the peaks, while with the HSE06 functional calculations, although providing correct optical band gaps, leads to the shift of the peaks approximately to 1 eV towards the high frequencies. Also, our results for cubic diamond and lonsdaleite are consistent with the earlier calculations in the work [32].

The predictions for allotropes C28, mtn, sic are presented in the Fig. 3 in comparison with diamond. The most of new allotropes (SiC12, H-Carbon, C28) demonstrate the very similar behavior of to diamond or lonsdaleite in the optical and UV region, so they do not lose the desirable optical parameters of diamond. In contrast, the mtn shows 2 times shorter and the smoothest peaks and has the smallest band gap in comparison to other allotropes, but the position of the peaks remains the same. Such a way, a presence of mtn in the polycrystalline sample can contribute a visual opacity.

The effect of the anisotropy of the optical properties for non-cubic structures is found to be small, so we do not show the dependence of the dielectric tensor from the crystal directions in the figures, but only the average values as defined by formula (2.6).

VII. CONCLUSION

In summary, the first-principles quantum-mechanical calculations have been performed to obtain the frequency spectra and optical properties of lowest-energy sp^3 carbon allotropes, such as: cubic diamond, lonsdaleite, SiC12, 4H-diamond, C28 and mtn. We have obtained Raman and IR spectra for all discussed allotropes and study their peculiarities. The electronic structure as well as the linear photon energy-dependent complex dielectric functions and related optical properties were computed. Our investigations are beneficial to the experimental search and to the practical applications of these hypothetic carbon allotropes in IR, visible and UV photonics [33,34].

VIII. ACKNOWLEDGEMENTS

The work was partially funded by the Ministry of Education and Science of Russia under Competitiveness Enhancement Program of Samara University for 2013-2020, project 3.5093.2017/8.9.

-
- [1] Adachi S. Optical constants of crystalline and amorphous semiconductors. New York: Springer Science and Business Media; 1999.
 - [2] Yang N. Novel aspects of diamond (Topics in Applied Physics, 121). Switzerland: Springer International Publishing; 2015.
 - [3] Zaitsev AM. Optical properties of diamond. Berlin: Springer-Verlag; 2001.
 - [4] Bundy FP, Kasper JS. Hexagonal Diamond A New Form of Carbon J Chem Phys 1967; 46: 3437-3446.
 - [5] Frondel C. and Marvin UB. Lonsdaleite, a Hexagonal Polymorph of Diamond. Nature 1967; 214: 587-589.
 - [6] Hirai H, Kenichi K. Modified phases of diamond formed under shock compression and rapid quenching. Science 1991; 253(5021): 772-774.
 - [7] Hongliang H, Sekine T, Kobayashi T. Hexagonal diamond synthesis on h-GaNh-GaN strained films. Appl Phys Lett 2002; 81: 610.
 - [8] Mao WL, Mao HK, Eng PJ, Trainor TP, Newville M, Kao CC, Heinz DL, Shu J, Meng Y and Hemley RJ. Bonding changes in compressed superhard graphite. Science 2003; 302: 425-427.
 - [9] Hoffmann R, Kabanov AA, Golov AA, Proserpio DM. Angew Chem Int Ed 2016; 55: 10962-10977.
 - [10] Hu M, Huang Q et al. Superhard and high-strength yne-diamond semimetals. Diamond and Related Materials. 2014; 46(0): 15-20.
 - [11] Wang JT, Chen C. Mechanism for direct conversion of graphite to diamond. Phys Rev B 2011; 84(1): 012102.
 - [12] Baburin IA, Proserpio DM, Saleev VA, Shipilova AV. From zeolite nets to sp^3 carbon allotropes: A topology-based multiscale theoretical study. Physical Chemistry Chemical Physics. 2015; 17(2): 1332-1338.

- [13] Nesper R., Vogel K, et al. Hypothetical Carbon Modifications Derived from Zeolite Frameworks. *Angewandte Chemie-International Edition in English* 1993; 32(5): 701-703.
- [14] Hohenberg P, Kohn W. Inhomogeneous Electron Gas. *Phys Rev* 1964; 136: B864-B871.
- [15] Kohn W, Sham LJ. Self-Consistent Equations Including Exchange and Correlation Effects. *Phys Rev* 1965; 140: A1133-A1138.
- [16] Dovesi R et al. A program for the ab initio investigation of crystalline solids. *Int J Quantum Chem* 2014; 114: 1287-1317.
- [17] Kresse G, Furthmüller J. Efficient iterative schemes for ab initio total-energy calculations using a plane-wave basis set. *Phys Rev B* 1996; 54:11169-11186.
- [18] Pascale F, Zicovich-Wilson CM, Lopez F, Civalleri B, Orlando R, Dovesi R. The calculation of the vibration frequencies of crystalline compounds and its implementation in the CRYSTAL code. *J Comput Chem* 2004; 25: 888-897.
- [19] Maschio L, Kirtman B, Rérat M, Orlando R, and Dovesi R. Ab initio analytical Raman intensities for periodic systems through a coupled perturbed Hartree-Fock/Kohn-Sham method in an atomic orbital basis. *J Chem Phys* 2013; 139: 164101.
- [20] Ferrero M, Rérat M, Orlando R, Dovesi R. The calculation of static polarizabilities in 1-3D periodic compounds. The implementation in the CRYSTAL code. *J Comput Chem* 2008; 29: 1450-1459.
- [21] Perdew JP, Burke K, Ernzerhof M. Generalized Gradient Approximation Made Simple. *Phys Rev Lett* 1996; 77: 3865 -3868.
- [22] Peintinger MF, Oliveira DV, Bredow T. Consistent Gaussian Basis Sets of Triple-Zeta Valence with Polarization Quality for Solid-State Calculations. *J Comp Chem* 2013; 34: 451-459.
- [23] Becke AD. Density-functional thermochemistry. 3. The role of exact exchange. *J Chem Phys* 1993; 98: 5648-5652.
- [24] Gordon MS, Binkley JS, Pople JA, Pietro WJ, Hehre WJ. Self-Consistent Molecular Orbital Methods. 22. Small Split-Valence Basis Sets for Second-Row Elements. *J Am Chem Soc* 1982; 104: 2797-2803.
- [25] Baima J, Zelferino A, Olivero P, Erba A, Dovesi R. Raman spectroscopic features of the neutral vacancy in diamond from ab initio quantum-mechanical calculations. *Phys Chem Chem Phys* 2016; 18: 1961-1968.
- [26] Heyd J, Scuseria GE, Ernzerhof M. Hybrid functionals on a screened Coulomb potential. *J.*

- Chem. Phys. 2006; 77: 219906.
- [27] Isaenko S, Shumilova T. Thermostimulated Raman spectrum dynamics of lonsdaleite. *Geoph Res Abs* 2012; 14:608.
 - [28] Goryainov SV, Likhacheva AY, et al. Raman identification of lonsdaleite in Popigai impactites. *J Raman Spectrosc* 2014; 45:305-313.
 - [29] Filik J, Harvey JN, Allan NL, May PW. Raman spectroscopy of nanocrystalline diamond: An ab initio approach. *Phys Rev B* 2006; 74:035423.
 - [30] Wu BR, Xu J. Total energy calculations of the lattice properties of cubic and hexagonal diamond. *Phys Rev B* 1998; 57: 13355-13359.
 - [31] Denisov VN, Mavrin BN, et. al. First-principles, UV Raman, X-ray diffraction and TEM study of the structure and lattice dynamics of the diamond-lonsdaleite system. *Diamond and Related Materials* 2011; 20:951-953.
 - [32] Wang Z, Zhang RJ, Zheng YX, et al. Electronic and optical properties of novel carbon allotropes. *Carbon* 2016; 101: 77-85.
 - [33] Kaminskii AA, Ralchenko VG, Yoneda H, Bolshakov AP, Inyushkin AV. Stimulated Raman scattering-active isotopically pure ^{12}C and ^{13}C diamond crystals: A milestone in the development of diamond photonics. *JETP Letters* 2016; 104(5): 347352.
 - [34] Salvatori S, Girolami M, Oliva P, Conte G, Bolshakov A, Ralchenko V, Konov V. Diamond device architectures for UV laser monitoring. *Laser Phys.* 2016; 26: 084005.

TABLE I: Lattice parameters for carbon allotropes calculated with POB-TZVP basis set and PBE exchange-correlation functional.

Structure	N	a, Å	b, Å	c, Å	Atomic positions
diamond	227	3.569			(0.125, 0.125, 0.125)
lonsdaleite	194	2.507		4.169	(0.333, 0.667, 0.062)
mtn	227	9.625			(0.880, 0.067, 0.683) (0.125, 0.125, 0.125) (0.033, 0.033, 0.716)
SiC12	166	2.511		24.822	(0.667, 0.333, 0.740) (0.667, 0.333, 0.572) (0.667, 0.333, 0.511) (0.000, 0.000, 0.656)
C28	55	7.298	7.728	2.535	(0.328, 0.039, 0.000) (0.376, 0.151, 0.500) (0.207, 0.270, 0.5000) (0.239, 0.384, 0.000) (0.015, 0.196, 0.500) (0.460, 0.408, 0.000)
4H-diamond	195	2.534		8.355	(0.000, 0.000, 0.093) (0.667, 0.333, 0.155)

TABLE II: Lattice parameters for carbon allotropes calculated with Poples 6-21 basis set and B3LYP exchange-correlation functional.

Structure	N	a, Å	b, Å	c, Å	Atomic positions
diamond	227	3.594			(0.125, 0.125, 0.125)
lonsdaleite	194	2.527		4.205	(0.333, 0.667, 0.062)
mtn	227	9.688			(0.880, 0.067, 0.683) (0.125, 0.125, 0.125) (0.033, 0.033, 0.716)
SiC12	166	2.534		25.067	(0.333, 0.667, 0.073) (0.333, 0.667, 0.916) (0.333, 0.667, 0.000) (0.667, 0.333, 0.656)
C28	55	7.301	7.735	2.538	(0.398, 0.039, 0.000) (0.376, 0.151, 0.500) (0.268, 0.270, 0.5000) (0.239, 0.384, 0.000) (0.015, 0.196, 0.500) (0.460, 0.408, 0.000)
4H-diamond	195	2.513		8.266	(0.000, 0.000, 0.093) (0.667, 0.333, 0.156)

TABLE III: Energy difference per atom relatively diamond, density and bulk modulus of the allotrope (PBE, POB-TZVP).

Structure	$\Delta E/atom$, eV	ρ , g/cm ³	B , GPa
diamond	0.00	3.51	443
4H-diamond	0.01	3.61	445
SiC12	0.01	3.53	444
lonsdaleite	0.03	3.52	445
C28	0.07	3.35	427
mtn	0.11	3.06	383

TABLE IV: Energy difference per atom relatively diamond, density and bulk modulus of the allotrope (B3LYP, 6-21G).

Structure	$\Delta E/atom$, eV	ρ , g/cm ³	B , GPa
diamond	0.00	3.43	428
4H-diamond	0.01	3.53	429
SiC12	0.01	3.43	428
lonsdaleite	0.03	3.43	429
C28	0.07	3.37	413
mtn	0.08	2.98	371

TABLE V: High-frequency refractive indices along the different directions.

Structure \ Basis set	POB-TZVP, PBE	Pople-6-21G, B3LYP
	$n_{xx}; n_{yy}; n_{zz}$	$n_{xx}; n_{yy}; n_{zz}$
diamond	2.40; 2.40; 2.40	2.34; 2.34; 2.34
4H-diamond	2.37; 2.37; 2.43	2.32; 2.32; 2.34
SiC12	2.38; 2.38; 2.42	2.32; 2.32; 2.36
lonsdaleite	2.36; 2.36; 2.40	2.30; 2.30; 2.36
C28	2.35; 2.38; 2.43	2.29; 2.32; 2.36
mtn	2.11; 2.11; 2.11	2.10; 2.10; 2.10

TABLE VI: IR active modes (Pople-6-21G, B3LYP).

Structure	IR active modes
SiC12	$E_u(425)$, $E_u(578)$, $A_{2u}(728)$, $A_{2u}(1075)$, $E_u(1271)$, $A_{2u}(1330)$
4H-diamond	$E_{1u}(1248)$, $A_{2u}(1316)$
C28	$B_{2u}(443)$, $B_{2u}(539)$, $B_{3u}(547)$, $B_{1u}(586)$, $B_{1u}(719)$, $B_{3u}(742)$, $B_{2u}(786)$, $B_{2u}(862)$, $B_{3u}(878)$, $B_{2u}(962)$, $B_{3u}(1000)$, $B_{2u}(1002)$, $B_{1u}(1071)$, $B_{3u}(1074)$, $B_{3u}(1172)$, $B_{3u}(1203)$, $B_{2u}(1211)$, $B_{1u}(1220)$, $B_{2u}(1239)$, $B_{1u}(1260)$, $B_{2u}(1278)$, $B_{3u}(1279)$, $B_{3u}(1298)$, $B_{3u}(1352)$, $B_{2u}(1356)$, $B_{2u}(1400)$
mtn	$F_{1u}(735)$, $F_{1u}(871)$, $F_{1u}(891)$, $F_{1u}(1059)$, $F_{1u}(1144)$, $F_{1u}(1223)$

TABLE VII: Band gaps for carbon allotropes.

Structure	PBE, indirect	HSE06, indirect	PBE, direct	HSE06, indirect
diamond	4.67	5.38	5.64	7.04
lonsdaleite	3.34	4.91	4.96	6.37
mtn	3.76	5.09	3.76	5.03
SiC12	4.44	5.64	5.25	6.65
C28	4.77	5.96	4.77	6.06
4H-diamond	4.53	5.73	5.29	6.68

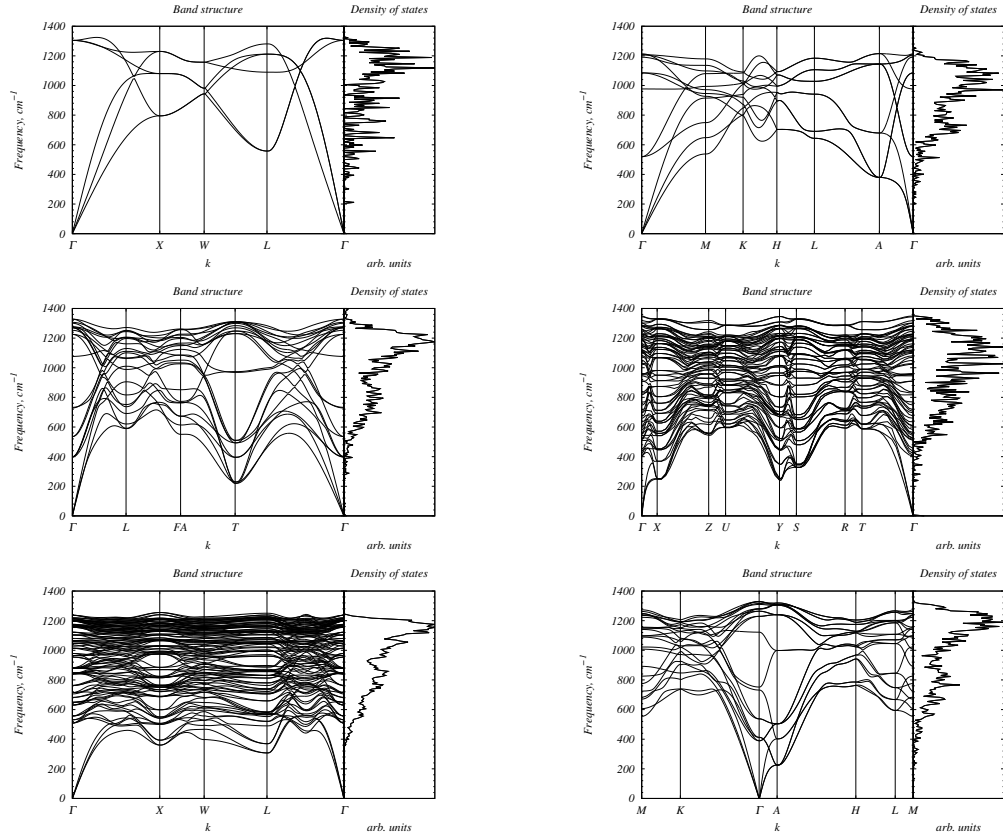


FIG. 1: Phonon band structures and density of states of allotropes. Left column: diamond, SiC12, and mtn. Right column: lonsdaleite, C28, and 4H-diamond

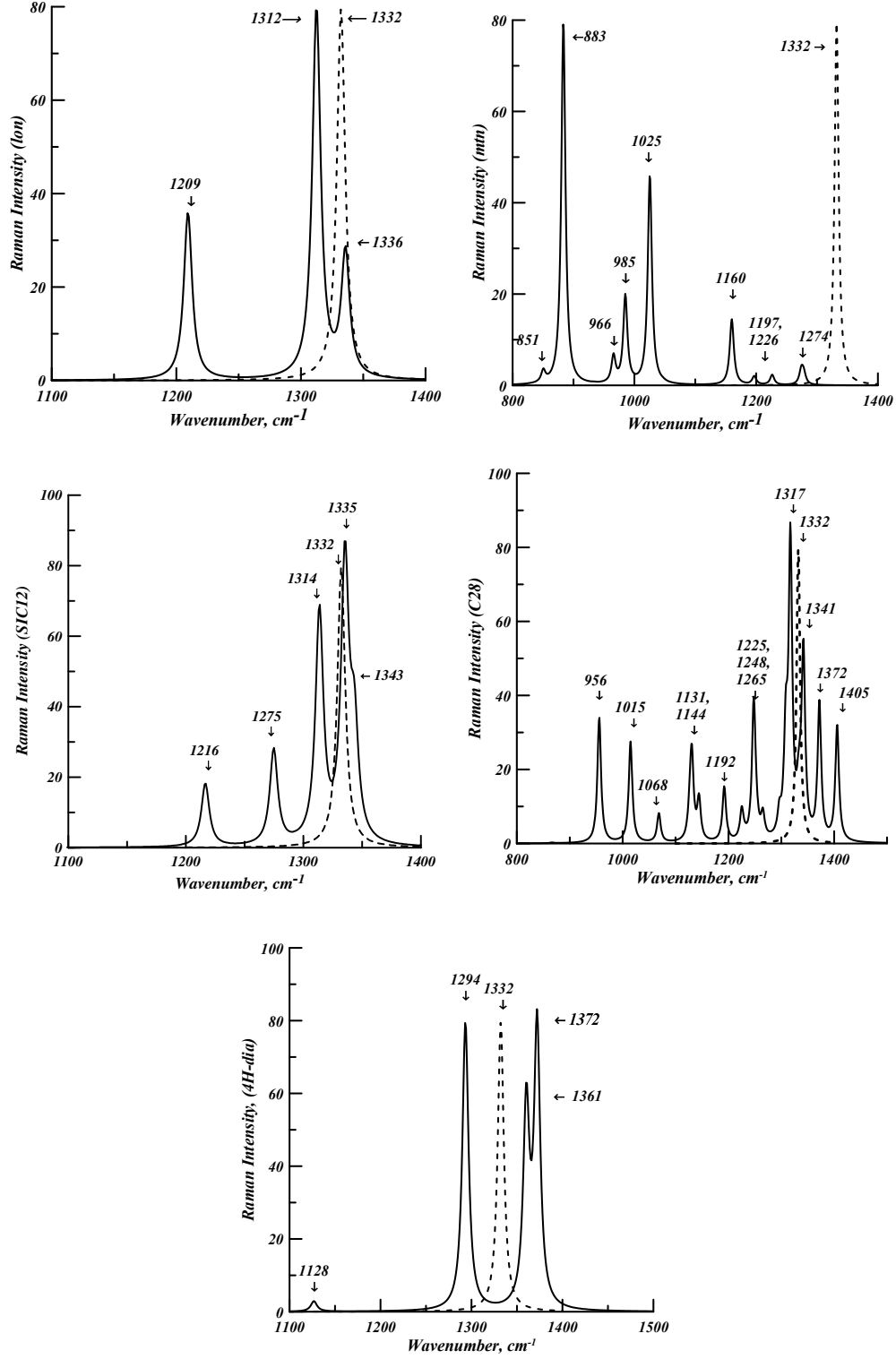


FIG. 2: Raman shift spectra in arbitrary units for carbon allotropes: a) lonsdaleite, b) mtn, c) SiC12, d) C28, e) 4H-diamond. The peak at the 1332 cm^{-1} in all panels corresponds cubic diamond.

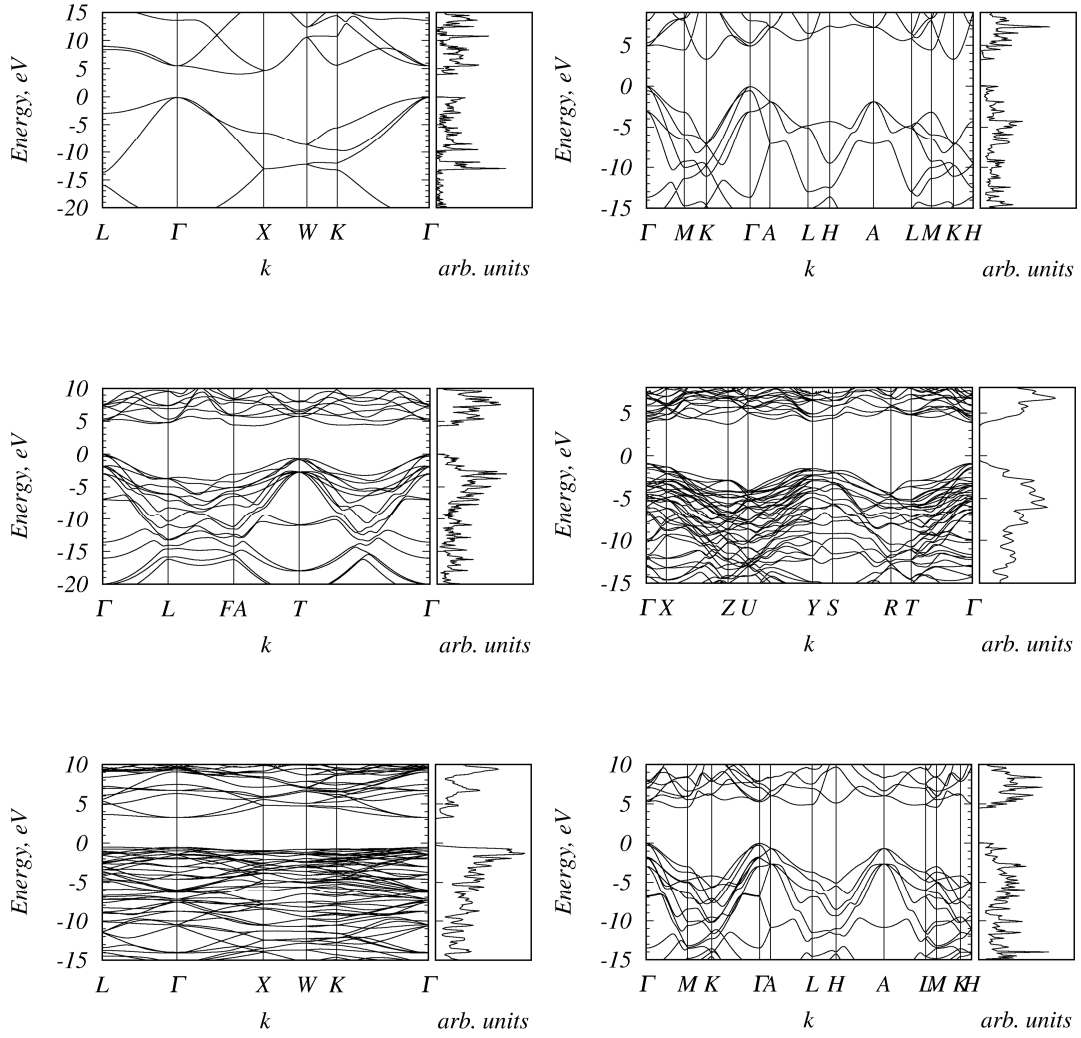


FIG. 3: Electronic band structures and density of states of allotropes. Left column: diamond, SiC12, and mtn. Right column: lonsdaleite, C28, and 4H-diamond

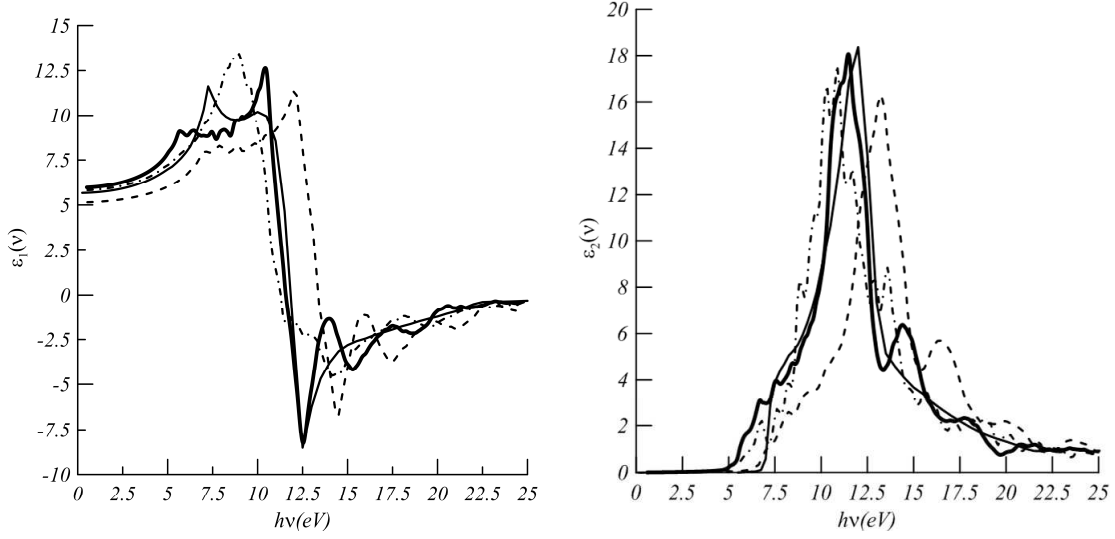


FIG. 4: Real (a) and imaginary (b) dielectric functions: solid line - experiment for cubic diamond, bold solid line - prediction for cubic diamond with PBE exchange-correlation functional, dashed line - prediction for cubic diamond with HSE06 functional, dash-dotted line - lonsdaleite with PBE functional.

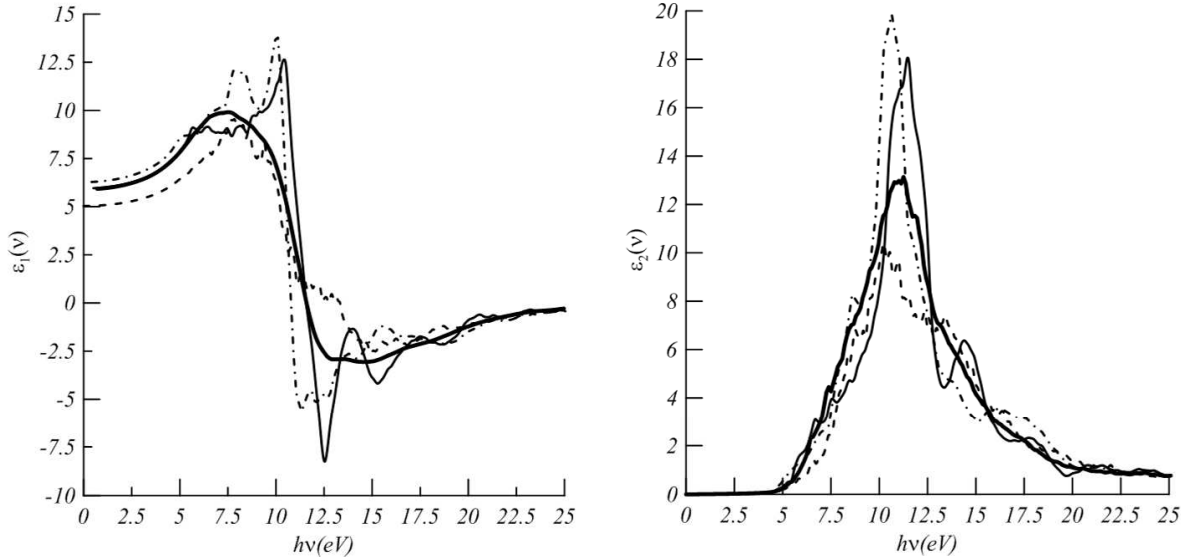


FIG. 5: Real (a) and imaginary (b) dielectric functions predicted for carbon allotropes with PBE functional: solid line - cubic diamond, bold solid line - C28, dashed line - mtn, dash-dotted line - SiC12.